13th International Symposium on Turbulence and Shear Flow Phenomena (TSFP13)
Montreal, Canada, June 25-28, 2024

SPACING RATIO EFFECTS ON THE UNSTEADY WAKE DYNAMICS OF UNEQUAL-HEIGHT TANDEM CIRCULAR CYLINDERS

Newton F. Ouedraogo
Department of Mechanical, Industrial and Aerospace Engineering
Concordia University
Montreal, QC, Canada, H3G 1M8
n_ouedr@live.concordia.ca

Ashim Chhetri
Department of Mechanical, Industrial and Aerospace Engineering
Concordia University
Montreal, QC, Canada, H3G 1M8
a_chhe@live.concordia.ca

Ebenezer E. Essel
Department of Mechanical, Industrial and Aerospace Engineering
Concordia University
Montreal, QC, Canada, H3G 1M8
ebenezer.essel@concordia.ca

ABSTRACT

Time-resolved particle image velocimetry is used to investigate the effects of spacing ratio on the unsteady wake dynamics of unequal-height tandem cylinders placed in a turbulent boundary layer (TBL). The aspect ratios of the finite wall mounted cylinders (FWMCs) were set to maintain a height ratio of 0.75, with the upstream cylinder (UC) having an aspect ratio of $h/d = 5.3$ while that of the downstream cylinder (DC) was $H/d = 7.0$, where h and H represent the height of the UC and DC, respectively, and d the diameter of the cylinders. The Reynolds number based on the cylinder diameter was $Re = 5540$, and the submergence ratio was $\delta/H = 1.2$, where δ is the thickness of the TBL. Three spacing ratios ($s/d = 2, 4$ and 6) obtained by varying the centre-to-centre distance (s) were used to investigate the extended body, reattachment, and co-shedding regimes of the tandem FWMCs. The three test cases, denoted as SR2, SR4 and SR6, respectively were compared to a single cylinder (SC) identical to the DC. The results showed that in the gap region, SR2 only displayed a downwash motion while SR4 and SR6 exhibited both downwash and upwash motions. Behind the DC, the reverse flow region was considerably reduced in the sheltered portion compared to the SC. The Reynolds stresses, production terms, and vortex dynamics analyzed using frequency spectra and spectral proper orthogonal decomposition (SPOD) were significantly influenced by the degree of sheltering induced by the spacing ratio.

INTRODUCTION

Flow past multiple finite wall-mounted cylinders (FWMCs) is encountered in diverse environmental and engineering applications. Examples include atmospheric boundary layer over buildings, chimney stacks, and wind turbines. Flow past multiple cylinders is characterized by unsteady three-dimensional flow features including flow separation and reattachment, quasi-periodic expansion and contraction (i.e., pumping motion) of recirculation bubbles, wake interference, tip and base vortices, and vortex shedding. Depending on the applications, the flow features may have positive or negative impacts. For example, vortex shedding on cylindrical structures may induce unsteady aerodynamic loads that may lead to flow-induced vibrations, acoustic noise, and fatigue failure. On the other hand, wake interference due to the position of a downstream structure in the wake of an upstream body induces a sheltering effect, leading to significant drag reduction for the downstream cylinder (Hamed et al. 2019; Sumner and Reitenbach 2019). Two cylinders arranged inline, side by side, or staggered represent simplified configurations that are often used to improve physical insights of the salient features of multiple FWMCs.

For two inline (i.e., tandem) two-dimensional (2D) cylinders, the center-to-center spacing (s) between the cylinders is used to categorize the flow into three main regimes: extended-body regime ($s/d \leq 2$, where d is the diameter of the cylinders), reattachment regime ($s/d \in [2,5]$), and co-shedding regime ($s/d \geq 5$) as shown by figure 1 (Zhou and Yiu, 2006). For extended-body regime, the separated shear layer of the upstream cylinder (UC) overshoots the downstream cylinder (DC), leaving a near-stagnant flow in the gap between the cylinders. In the case of the reattachment regime, the separated shear layers from the UC reattach onto the frontal ($s/d \in [2,3]$) or the rear ($s/d \in [3,5]$) surface of the DC, forming a quasi-steady gap flow. For the co-shedding regime, shedding occurs independently on each cylinder, resulting in a highly unsteady gap flow.

The flow regimes of tandem FWMCs depend on other important parameters including height ratio ($HR = h/H$, where h and H are the heights of the UC and DC, respectively), aspect ratio ($AR = h/d$ or H/d), submergence ratio (δ/H, where δ is the boundary layer thickness), Reynolds number and the turbulence intensity. Unequal-height tandem cylinders ($HR \neq 1$) exhibit a more complex topology compared to

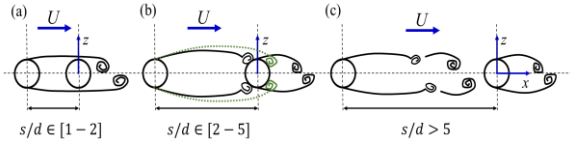

Figure 1. (a) Schematic of the flow regimes of tandem cylinders: extended body regime ($s/d \leq 2$), (b) reattachment regime ($s/d \in [2,5]$) and (c) co-shedding regime ($s/d \geq 5$).

identical height cylinder due to the impact of partial or complete sheltering of the downstream cylinder. However, the unsteady wake characteristics of unequal-height tandem cylinders are not well-understood, despite their prevalence in many engineering applications such as cluster of low and high-rise buildings and offshore structures.

Hamed et al. (2019) used a particle image velocimetry (PIV) to study the time-averaged flow field of low aspect ratio cylinders ($H/d = 2.5$) arranged inline in a thick turbulent boundary layer (TBL), and found that the degree of sheltering decreases with decreasing height ratio and increasing spacing ratio. Essel et al., (2023) showed that an increase in height ratio for a fixed spacing ratio ($s/d = 4$) significantly enhanced the degree of sheltering and modified the vortex shedding of the DC compared to an isolated single cylinder.

This paper investigates the unsteady wake dynamics of unequal-height tandem FWMCs fully submerged in a TBL ($\delta/H = 1.2$). Essel et al., (2023) and Hamed et al., (2019) reported a strong influence of sheltering on the wake dynamics of the unequal-height FWMCs and a lock-in pumping motion and vortex shedding at $s/d = 4$ for $h/H = 0.75$, therefore, a similar height ratio was selected for the present study. The spacing ratio effect was investigated using three spacing ratios ($s/d = 2, 4$ and 6) mimicking the three regimes observed for 2D tandem cylinders, and measurements were also performed for an isolated single cylinder to facilitate comparison of the wake characteristics.

EXPERIMENTAL SETUP & PROCEDURE

The experiments were performed in an open recirculating water channel facility equipped with a time-resolved particle image velocimetry (TR-PIV) system. The flow was driven by a 30-kW variable-speed drive pump through a flow conditioning unit before entering the transparent acrylic test section. The test section is 6000 mm long with a rectangular cross-section of 60 mm × 45 mm (width × height). Figure 1 shows a schematic drawing of the experimental setup with the two unequal cylinders arranged in tandem. The cylinders used were smooth round acrylic rods of diameter, $d = 12.7$ mm, and were vertically mounted with screws on a flat acrylic plate lining the entire floor of the test section. The origin of the left-handed Cartesian coordinate is located at the center of the DC and mid-span ($z/d = 0$) of the channel. The height ratio was fixed at 75% based on high aspect ratios of $h/d = 5.3$ and $H/d = 7$ for the UC and DC, respectively. The submergence ratio is $\delta/H = 1.2$. The freestream velocity was $U_\infty = 0.436$ m s^{-1} and the Reynolds number ($Re = U_\infty d/\nu$) was 5540. Three spacings ratios of $s/d = 2, 4$ and 6 were investigated, denoted as SR2, SR4, and SR6, for simplicity. For comparison, measurements were also conducted for a baseline case where the UC was removed, denoted as SC.

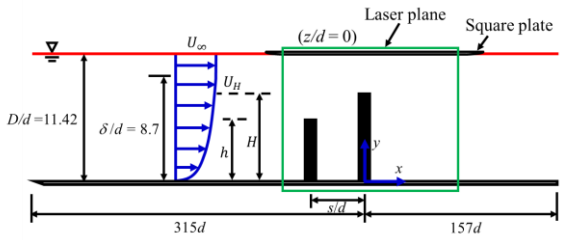

Figure 2. Schematic of the experimental setup for the tandem cylinders, the approach flow and field of view.

The velocity fields were measured using a planar TR-PIV system. The flow was seeded with 10 μm silver-coated hollow glass spheres of a specific gravity of 1.4. A high-speed 12-bit CMOS camera was used to capture instantaneous images of the flow illuminated with a dual-cavity high-speed pulsed Nd:YLF laser. For each test case, measurements were acquired in the *x*-*y* plane at the symmetry plane ($z/d = 0$) of the cylinders. A sample size of 48000 images were acquired for each test case in eight batches of 6000 images/batch at a sampling frequency of $f_{sp} = 1000\ Hz$. Based on the vortex shedding frequency at the mid-height of the SC, the total sampling time of $T = 48s$ corresponds to 264 cycles, ensuring statistical convergence of the spectral quantities reported herein.

RESULTS AND DISCUSSION

Mean Flow and Turbulence Statistics

Figure 3 shows contours of the wall-normal mean velocities with the mean streamlines superimposed for the SC and the unequal-height tandem cylinders (SR2, SR4 and SR6). In each plot, the reverse flow region ($U < 0$) is demarcated using the contour line of 50% forward fraction flow ($\gamma = 0.5$). The red dot represents the saddle point while the contour line of $U/U_H = 1$ is used to highlight the portion of the TBL that directly interacts with the cylinders. In the wake of the SC, tip vortices from the free end of the cylinder generates a strong downwash that clashes with a strong upwash from the base of the cylinder. This results in the wake exhibiting a quadrupole structure with the saddle point located close to the mid-height ($y/d = 4$) of the cylinder. In contrast to the present results, Hamed et al. (2019) observed a dipole structure behind the SC and this disparity is attributed to the higher AR in the present study. For the tandem cylinders, the wake structure of the DC is considerably altered compared to that of the SC. Particularly, the origin of the upwash moves upwards toward the free end of the DC along with the saddle point and is accompanied by a strong decrease of reverse flow region in the sheltered portion. The gap region is characterized by an enhanced downwash whose strength decreases with increasing spacing ratio. For SR2, the close proximity of the UC to the DC prevents the generation of an upwash flow and allows the deflected downwash flow to reattach onto the UC causing the reverse flow region to split in two portions. With increasing spacing ratio, the upwash in the gap region gradually increases allowing the saddle point behind the UC to move up in the wall-normal direction. The wake structure and reverse flow region of the UC for SR6 is akin to that of the SC. Behind UC, the length of the reverse flow region determined as the streamwise distance from the rear end surface of the cylinder to the furthest location of the isopleth of 50% forward flow fraction increased from $0.9d$ to $3d$ as the spacing ratio is increased from SR2 to SR4, but reduced to $2.2d$ for SR6. In contrast to the UC, behind the DC, the length of the reverse flow region, $1.85 \pm 0.15d$, is independent of aspect ratio, as the region is enlarged in the unsheltered portion of the DC. For all the tandem cases, the length of the reverse flow region for SC, i.e., $2.3d$, is larger than that of the DC.

Profiles of Reynolds normal and shear stresses along with the production term of turbulent kinetic energy are shown in figure 4. The profiles were extracted in the gap region $1d$ behind the center of UC (i.e., $x^*/d = 1$) and $1, 2$ and $6d$ behind DC/SC (i.e., x/d =1, 2 and 6). In the gap region, the normal stresses are

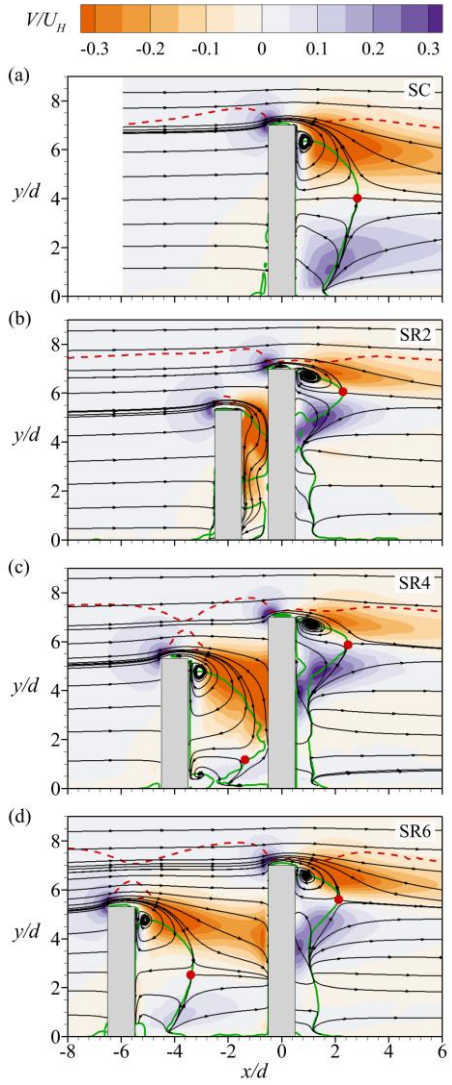

Figure 3. Contour of wall-normal mean velocity for (a) SC, (b) SR2, (c) SR4 and (d) SR6. Superimposed are the mean streamlines and the saddle point indicated by the red dots. The green solid line represents the isopleth of 50% forward-flow fraction while the red dashed line is the isopleth of $U/U_H = 1$.

more pronounced below the free end of the UC ($y/d \leq 5.3$) for SR2 due to the strong downwash and blockage by DC. Behind DC at $x/d = 1$, SR2 also exhibits higher normal stresses when compared to the other test cases, which is attributed to the influence of the spanwise separated shear layers from UC that overshoots DC. Further downstream ($x/d = 2$), SR6 displays higher peaks of streamwise Reynolds normal stress while the profiles of the wall-normal Reynolds normal stress are comparable to the other test cases. For $x/d \geq 6$, the profiles of the normal stresses are independent of the test case.

Figure 4(c) shows the Reynolds shear stress where, based on the orientation of the shear layer, a positive $-\langle uv \rangle$ is associated with downwash flow and negative $-\langle uv \rangle$ for upwash flow. However, the profiles at $x^*/d = 1$ for SR2 shows negative $-\langle uv \rangle$, despite the presence of a strong downwash in the gap region. Based on the production term of the transport equation of $-\langle uv \rangle$, it was found that the deflected downwash from DC that impinges on the UC enhanced the term $\left(-\langle uu \rangle \frac{\partial V}{\partial x}\right)$ leading to

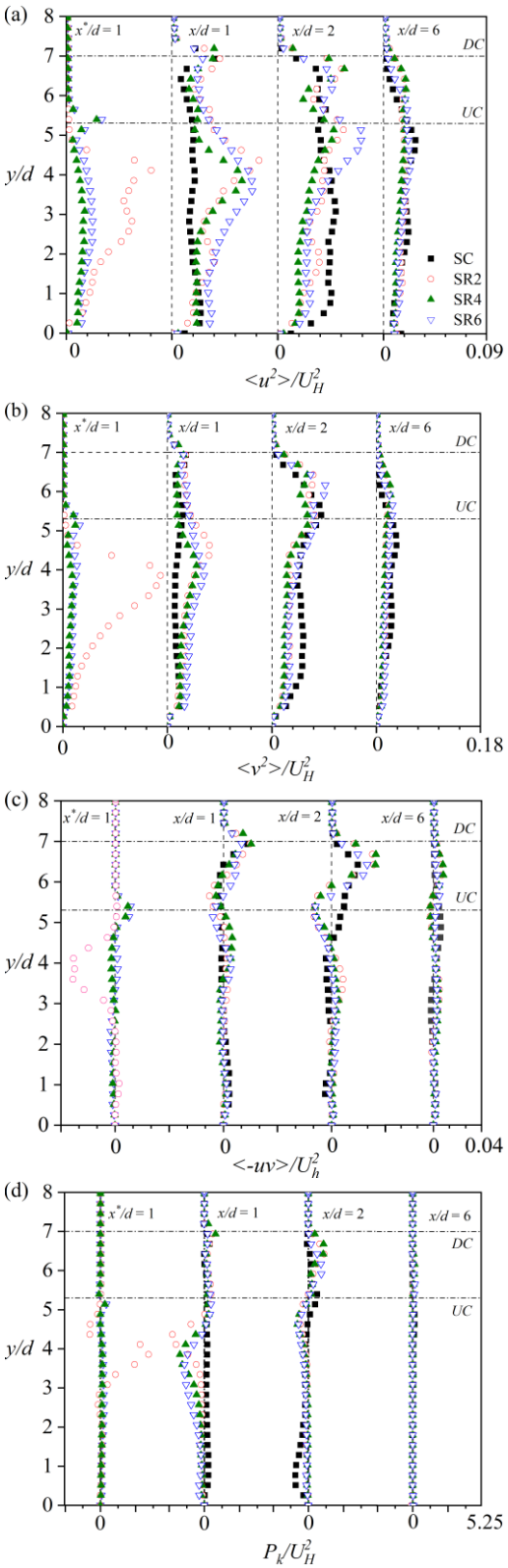

Figure 4. Profile of (a) streamwise and (b) wall-normal Reynolds normal stress, (c) Reynolds shear stress and (d) production term of turbulent kinetic energy at selected streamwise locations behind the UC ($x^*/d = 1$) and DC ($x/d = 1, 2$ and 6). horizontal dash line represents the normalized height of UC and DC.

negative $-\langle uv \rangle$ production in that region (Ouedraogo and Essel, 2023). Behind the SC, the Reynolds shear stress is enhanced only near the free end with positive $-\langle uv \rangle$. In contrast to the SC, the downstream region behind the DC exhibits an alternating behavior with an enhanced negative $-\langle uv \rangle$ for $y/d = 5.3$ and positive $-\langle uv \rangle$ close to the free end of the DC. The enhanced negative $-\langle uv \rangle$ is attributed to induced upwash behind DC.

To investigate the effect of the spacing ratio on the production of turbulent kinetic energy, figure 4 (d) shows profile of the production term of the transport equation of TKE (P_k). The production term of the TKE transport equation is given as

$$P_k = \frac{1}{2}(P_{uu} + P_{vv}) \tag{1}$$

where, P_{uu} and P_{vv} are determined as follows based on planar PIV measurement at the centerline of the cylinders

$$P_{uu} = -2\left(\overline{u^2}\frac{\partial \bar{U}}{\partial x} + \overline{uv}\frac{\partial U}{\partial y}\right) \tag{2}$$

$$P_{vv} = -2\left(\overline{v^2}\frac{\partial \bar{V}}{\partial y} + \overline{uv}\frac{\partial V}{\partial x}\right) \tag{3}$$

The production term P_{vv} was found to be the dominant source for P_k for all the test cases, which is uncommon for classical shear flows, e.g. turbulent boundary layers. In the gap region, SR2 has the highest peak for P_k resulting from a strong energy source term P_{vv} suppressing the energy sink from P_{uu}. Behind DC at $x/d = 1$ and 2, in the sheltered portion, the production term is negative as both of the contributors (P_{uu} and P_{vv}) acts as energy sinks. Meanwhile, for the unsheltered portion, the production term is positive for all the test cases due to the strong downwash and induced upwash that enhances P_{uu} (major contributor) and P_{vv}. In contrast to the DC of the tandem cylinders, the SC is less energetic as the profiles show weaker production of TKE.

Figure 5 shows the contours of the triple correlation term $\langle k_v \rangle$ (eqn. 4). Along with $\langle k_u \rangle$ (eqn. 5) (contours not shown for brevity), their gradients represent the turbulence diffusion term of the transport equation of TKE. These terms are expressed as follows

$$\langle k_v \rangle = \frac{1}{2}\left(\overline{v'}^3 + \overline{u'}^2\overline{v'}\right) \tag{4}$$

$$\langle k_u \rangle = \frac{1}{2}\left(\overline{u'}^3 + \overline{u'}\overline{v'}^2\right) \tag{5}$$

A positive value of $\langle k_v \rangle$ is associated with the transport of TKE in the upward direction while a negative value is associated with the transport in the downward direction. Also, a positive value of $\langle k_u \rangle$ is associated with transport of TKE by high-momentum fluid while negative value represents transport by low-momentum fluid. Behind the UC and DC/SC, the downwash shear layers are associated with positive $\langle k_v \rangle$ and negative $\langle k_u \rangle$ suggesting upward diffusion of TKE by low-momentum fluid toward the free end of the cylinder, while the upwash shear layers are mostly associated with negative $\langle k_v \rangle$ and positive $\langle k_u \rangle$ indicating downward diffusion of TKE by high-momentum fluid. In the gap region, SR2 has the most intense region of $+\langle k_u \rangle$ and $-\langle k_u \rangle$, while the topology of $\langle k_v \rangle$ and $\langle k_u \rangle$ behind DC significantly depends on spacing ratio.

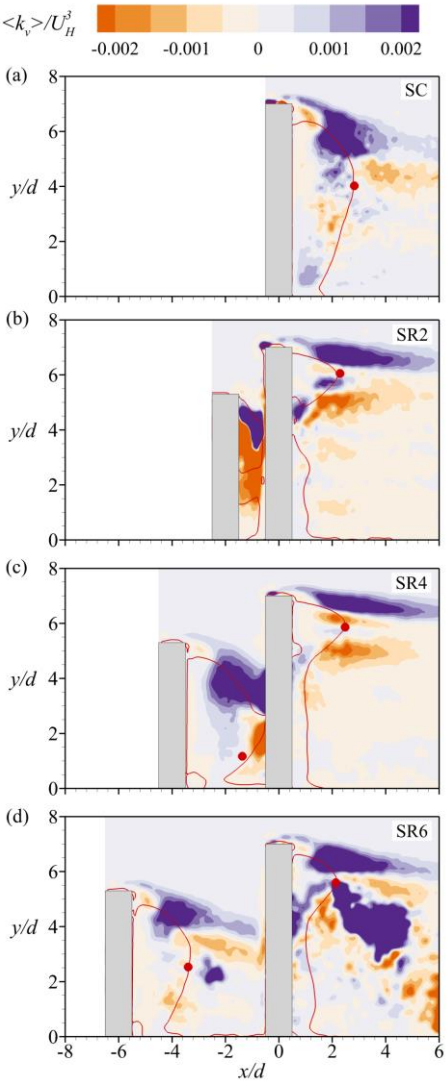

Figure 5. Contour of wall-normal component of turbulence diffusion $\langle k_v \rangle$ superimposed with the isopleth of 50% forward-flow fraction (red solid line) which bounds the reverse flow region and red dot represents the saddle point.

Spectral Analysis

The spectra of the wall-normal velocity fluctuations are shown by figure 6 to investigate the vortex shedding phenomena associated with the downwash motion in the symmetry plane of the cylinders. The profiles were extracted behind the UC at $x/d = -1$ for SR2 and SR4 and $x/d = -3$ for SR6 and behind the SC/DC at $x/d = 5$ and the wall-normal locations were set to coincide with the locations of maximum u_{rms}. For SR2, behind the UC, the downwash exhibits a low-frequency vortex shedding ($St = 0.056$) accompanied by a dominant second harmonic ($St = 0.117$). The vortex shedding frequency in the gap region is found to increase with increasing spacing ratio (i.e., $St = 0.249$ for SR4 and $St = 0.283$ for SR6) which are relatively higher than $St = 0.150$ reported by (Essel et al., 2023) for the spanwise vortex shedding of an isolated cylinder identical UC. In contrast to the SC showing a distinct peak at $St = 0.344$, the spectra of DC for the SR2-SR6 exhibit less pronounced peaks due to sheltering effects. Essel et al., (2021) reported $St \in [0.02,0.21]$ for spanwise plane located at y/d = 0.5, 3.5 and 6.5 which is relatively lower than the $St = 0.344$ depicted by the downwash.

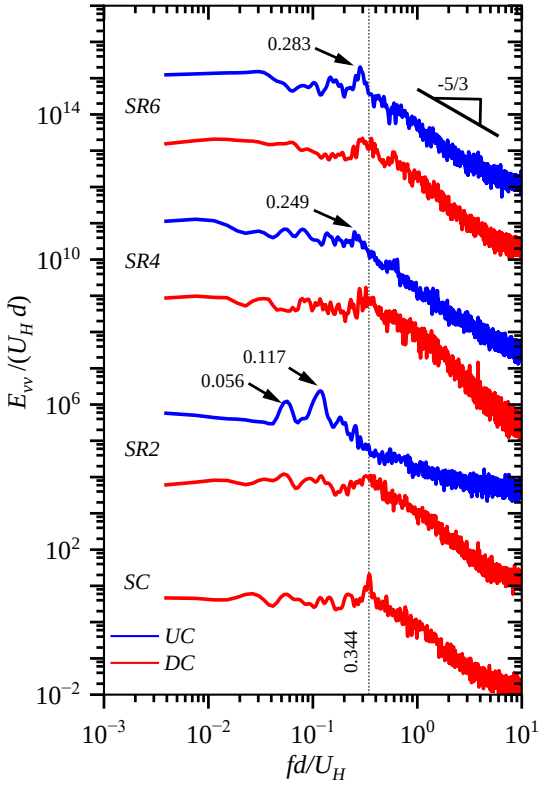

Figure 6. Spectra of the wall-normal velocity fluctuations behind the UC and SC/DC for each test case. For clarity, the spectra are offset arbitrarily.

Spectral Proper Orthogonal Decomposition

The spatio-temporal characteristics of the vortical structures are examined using spectral proper orthogonal decomposition (SPOD). The SPOD method extract the spatial energetic structures of the entire frequency domain and sorts them according to their advection frequency (Towne et al., 2018). In the framework of SPOD, a Fourier transform is applied to the time-resolved flow field. The Fourier transformed flow field is then decomposed into different mode using the POD technique. The fluctuating velocity component is then expressed as

$$\vartheta'(x,y,t) = \sum_{j=1}^{\infty}\sum_{m=1}^{\infty} \phi_j^m(x,y) a_j^m e^{-i\omega_j t} + c.c. \qquad (3.4)$$

where ϕ_j^m is the orthogonal set of spatial eigenfunctions (modes) and a_j^m their associated coefficients, and the wavenumber $\omega_j = 2\pi f_j$. Here the indices j and m represent the frequency and mode number while $i \equiv \sqrt{-1}$ and $c.c.$ denotes the complex conjugate. Here, the SPOD technique allows to study the effects of the spacing ratio on the energetic structures associated with vortex shedding in the symmetry plane of the cylinders.

The pre-multiplied energy spectra of the most energetic mode, Mode 1, is shown in figure 7. For all the test cases, the spectra are showing clear peaks at $St = 0.344, 0.117, 249$ and 0.287 for SC, SR2, SR4 and SR6, respectively which are similar to the Strouhal numbers observed in the downwash motion (see figure 6). This observation demonstrates that the vortex shedding from the UC is prominent and dictates the shedding motion of the DC.

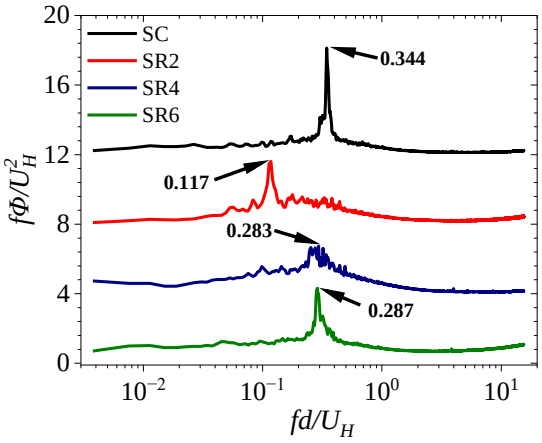

Figure 7. Premultiplied energy spectra of Mode 1 at the dominant Strouhal numbers for SC, SR2, SR4, and SR6.

Contours of the wall normal component ϕ_v of Mode 1 at the dominant Strouhal number of each test case are shown in figure 9. The large packet of alternating vortices is shed behind SC converges further downstream due to the influence of the upwash and downwash flows. In the gap region of SR2, the proximity of the DC prevents the vortices shed from the UC to develop. Behind the DC for SR2, larger vortices with irregular pattern are shed in a manner that is significantly different from SC, SR4 and SR6. This irregular pattern is attributed to the combined effects of spanwise vortices shed from the UC that overshoot the DC and vortices shed from the free end of the DC. As the spacing ratio increases, the shedding of alternate packets behind UC is enhanced and the larger spacing between the cylinders allows the vortices to evolve downstream in a more ordered pattern before interacting with the DC. Behind DC for SR4 and SR6, the packets of alternating vortices are observed mostly in the unsheltered portion with weaker vortices in the sheltered part.

CONCLUSION

Time-resolved PIV system was used to investigate the influence of spacing ratio on the unsteady wake characteristics of unequal-height tandem FWMCs. The cylinders of height ratio $h/H = 0.75$ were submerged in a boundary layer of thickness, $\delta/H = 1.2$ where h and H are the heights of the upstream (UC) and downstream (DC) cylinder, respectively and δ is the boundary layer thickness. Three spacing ratios, $s/d = 2, 4$ and 6 were studied to represent the three main flow regimes: extended body, reattachment, and co-shedding regimes, respectively.

The wake of the reference isolated cylinder (SC) with height similar to DC exhibited a quadrupole structure with saddle point near the mid-height. Introducing the UC, considerably reduced the reverse flow region behind the DC and shifted the saddle point to the unsheltered portion near the free end of the DC. In the gap between the cylinders, SR2 only showed a strong downwash, but SR4 and SR6 displayed both downwash and upwash flow that contributed to the enlargement of the reverse flow region behind the UC for these test cases.

The Reynolds normal stresses were found to be stronger for SR2 in the gap region due to strong downwash and close proximity of DC. However, behind DC, SR6 showed the largest Reynolds normal stresses. The production term of $\langle v^2 \rangle$ was the major contributor to the production of TKE in the gap region, while behind DC, the production term of $\langle u^2 \rangle$ dominates. In both

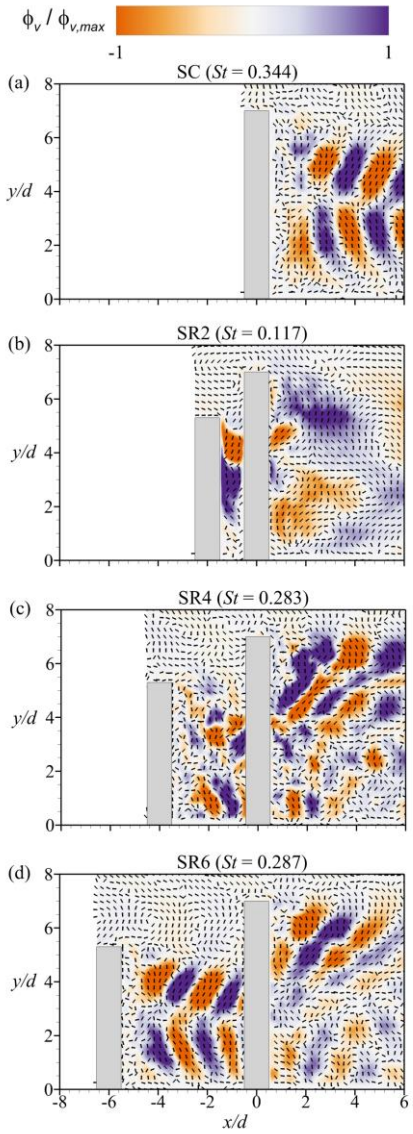

Figure 9. Contours of wall-normal (ϕ_v) components of Mode 1 at the dominant Strouhal numbers for SC, SR2, SR4, and SR6. The vectors of ϕ_u and ϕ_v are shown on each plot.

cases, the production of TKE decreases as spacing ratio increases. Meanwhile, the contributions of the triple correlations to turbulence diffusion increases with increasing spacing ratio.

As spacing ratio increased, the Strouhal number of the vortex shedding motion in the downwash flow behind the UC increased, as observed in the regular shedding pattern revealed by Mode 1 SPOD. Behind DC, the Strouhal number is lower than that of SC and independent of spacing ratio. Moreover, the vortex shedding was more pronounced in the unsheltered portion of DC and as spacing ratio increased.

REFERENCES

Crane, R. J., Popinhak, A. R., Martinuzzi, R. J., and Morton, C., 2022, "Tomographic piv investigation of vortex shedding topology for a cantilevered circular cylinder", *Journal of Fluid Mechanics*, Vol. 931, R1.

Essel, E. E., Balachandar, R., and Tachie, M. F., 2023, "Effects of sheltering on the unsteady wake dynamics of tandem cylinders mounted in a turbulent boundary layer", *Journal of Fluid Mechanics*, Vol. 954, A40.

Essel, E. E., Tachie, M. F., and Balachandar, R., 2021, "Time-resolved wake dynamics of finite wall-mounted circular cylinders submerged in a turbulent boundary layer", *Journal of Fluid Mechanics*, Vol. 917, A8.

Hamed, A. M., and Peterlein, A. M., 2020, "Turbulence structure of boundary layers perturbed by isolated and tandem roughness elements", *Journal of Turbulence*, Vol 21, pp. 17–33.

Hamed, A. M., Peterlein, A. M., and Randle, L. V, 2019, "Turbulent boundary layer perturbation by two wall-mounted cylindrical roughness elements arranged in tandem: Effects of spacing and height ratio", *Physics of Fluids*, Vol. 31.

Kim, T., and Christensen, K. T., 2018, "Flow interactions between streamwise-aligned tandem cylinders in turbulent channel flow", *AIAA Journal*, Vol 56, pp. 1421–1433.

Krajnović, S., 2011, "Flow around a tall finite cylinder explored by large eddy simulation", *Journal of Fluid Mechanics*, Vol. 676, pp. 294–317.

Palau-Salvador, G., Stoesser, T., and Rodi, W., 2008, "LES of the flow around two cylinders in tandem", *Journal of Fluids and Structures*, Vol. 24, pp. 1304–1312.

Papaioannou, G. V., Yue, D. K. P., Triantafyllou, M. S., and Karniadakis, G. E., 2006, "Three-dimensionality effects in flow around two tandem cylinders", *Journal of Fluid Mechanics*, Vol. 558, pp. 387–413.

Pearson, D. S., Goulart, P. J., and Ganapathisubramani, B., 2013, "Turbulent separation upstream of a forward-facing step", *Journal of Fluid Mechanics*, Vol. 724, pp. 284–304.

Porteous, R., Moreau, D. J., and Doolan, C. J., 2014, "A review of flow-induced noise from finite wall-mounted cylinders", *Journal of Fluids and Structures*, Vol. 51, pp. 240–254.

Sumner, D., and Li, H., 2014, "Wake interference effects for two surface-mounted finite cylinders in a tandem configuration", *Proceedings, of the ASME 2014 Pressure Vessels & Piping Conference*, Anaheim, California, USA, pp. PVP2014-28056.

Towne, A., Schmidt, O. T., and Colonius, T., 2018, "Spectral proper orthogonal decomposition and its relationship to dynamic mode decomposition and resolvent analysis", *Journal of Fluid Mechanics*, Vol. 847, pp. 821–867.

Zhou, Y., and Yiu, M. W., 2006, "Flow structure, momentum and heat transport in a two-tandem-cylinder wake", *Journal of Fluid Mechanics*, Vol. 548, pp. 17–48.